Magnetic properties of ferromagnetic materials produced by 3D multi-material printing

1st Nikolaus Trnka
Chemnitz Universiy of Technology
Electromagnetic Energy Conversion Systems and Drives
Chemnitz, Germany
trnka@hrz.tu-chemnitz.de

2nd Johannes Rudolph
Chemnitz Universiy of Technology
Electromagnetic Energy Conversion Systems and Drives
Chemnitz, Germany
johannes.rudolph@etit.tu-chemnitz.de

3rd Ralf Werner
Chemnitz Universiy of Technology
Electromagnetic Energy Conversion Systems and Drives
Chemnitz, Germany
ralf.werner@etit.tu-chemnitz.de

***Abstract*—In this paper, development of the magnetic properties of ferromagnetic material, used for the new 3D multi-material printing process (3DMMP) is shown. First the technology of the printing process as well as the measuring principle and the test bench are described. Furthermore, an overview of the material development is given and the measurement results are discussed. This is followed by the consideration of relevant influences for further development of the materials and comparison of the measured hysteresis loops with different standard materials.**

***Index Terms*—3D multi-material printing, magnetic properties, measurement, hysteresis, core losses**

I. 3D MULTI-MATERIAL PRINTING

'3D printing' covers a variety of different generative or additive manufacturing processes. Depending on the base material different manufacturing technologies are used. Powder bed based processes are e.g. laser melting or laser sintering, where shaping is realized through local melting of small metallic particles using a laser or electron beam [1], and binder jet printing, where the powder bed is agglutinated using a binder [2] [3]. More common are plastic-based 3D printers, which are increasingly being used in the private sector due to their low cost. These usually work using FDM (Fused Deposition Modeling) technology, in which a plastic filament is melted locally and extruded through a nozzle. There are also a large number of other processes which can be used to produce complex structures from various polymers, metals and ceramics. The main limitation of all these processes is that either only plastics can be processed or only one material can be used in the printing process. Although there have been some attempts to process several materials simultaneously using conventional methods [4] [5] [6], the choice is typically limited to one metal or ceramic powder.

A. Motivation to develop a multi-material 3D printing process

In view of the growing number of mobile applications and the expansion of electromobility in particular, there is a need for electrical machines with higher power density and increased overload capacity. The required higher current density in the machine leads to an increase in current heat losses, which are caused by the electrical resistance of the copper windings. The maximum operating temperature of electrical machines is generally limited by the thermal stability of the insulation materials. These are usually made of polymer-based materials that allow operating temperatures of approximately $180^\circ\,\mathrm{C} \ldots 200^\circ\,\mathrm{C}$. At the same time, these insulation materials are subject to a thermal aging process [7]. The substitution of polymer-based materials by ceramic insulations offers the possibility to overcome this limitation. Compared to insulation materials made of plastic with a thermal conductivity of approx. $0.5\,\mathrm{W/K{\cdot}m}$, ceramic materials have a thermal conductivity of $2 \ldots 5\,\mathrm{W/K{\cdot}m}$ for silicate ceramics and up to $30\,\mathrm{W/K{\cdot}m}$ for alumina ceramics [8]. Ceramic insulated wires are often too expensive and the processing too complex due to the sensitivity of the ceramic layer to small bending radii and mechanical stresses [9]. An alternative approach is the use of additive manufacturing, which eliminates the need for subsequent shaping of the ceramic-copper composite. The above-mentioned limitations of common printing methods lead to the development of an additive manufacturing process in order to be able to process metals (copper and iron) and ceramics in one process.

B. The procedure

3D multi-material printing (3DMMP) is characterized by the unique ability to use different materials in one printing process. In addition to mechanical properties, it is possible to realize properties required for electrical engineering, such as significant electrical conductivity, insulation capacity and the magnetizability of printed components. Highly viscous pastes are used, which are made of fine powders of the target materials and special binding additives. Structures are built up in layers by extruding the pastes through fine nozzles, see Fig. 1. After drying, the so-called green body already has a certain firmness, which allows post-processing. The printed body is then subjected to a thermal process for 6-14 hours with

978-1-7281-5635-4/20/$31.00 ©2020 IEEE

Authorized licensed use limited to: Middlesex University. Downloaded on September 03,2020 at 02:46:27 UTC from IEEE Xplore. Restrictions apply.

maximum temperature about melting temperature of copper in which the binding materials are removed and the particles melt together. Examples for these steps are shown in Fig. 2 By combining copper, ceramics and iron in one printing process, it is possible to produce not only ceramic-insulated thermal high-performance windings (e.g. tooth coils) [10] [11] but also entire electric motors [12]. In order to be able to predict the expected operating behaviour of machines produced by 3DMMP, knowledge of the magnetic properties of the printed ferromagnetic materials is necessary.

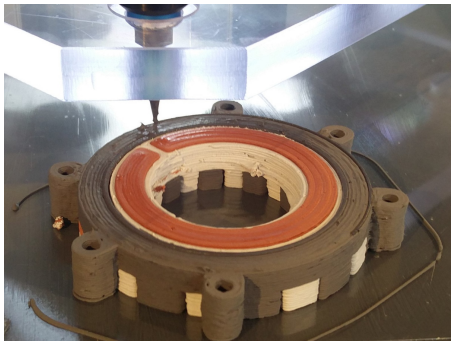

Fig. 1. Processing 3DMMP: entirely printed motor [12]

II. Determination of Magnetic Properties

Common principles for determining the magnetic properties of material samples use single sheets i.e. not closed magnetic circuits or samples which are designed as closed magnetic circuits. For this purpose, an Epstein frame is often used, in which a closed magnetic circuit is formed of individual metal strips. The procedure has various systematic errors [13], so ring samples are used as an alternative. These form a homogeneous, closed magnetic circuit. Some of the first measured samples are shown in Fig. 2.

A. Measuring principle

The measurement is based on the transformer principle and is performed on ring samples with a rectangular cross-section. The sample is equipped with two windings. One winding is used to magnetize the sample by applying an alternating current $i_1(t)$, that has to be measured over time. Assuming a constant sample cross section, the magnetic field strength as a function of time can be calculated.

$$H(t) = i_1(t) \cdot \frac{N_1}{l_{\mathrm{mag}}} \tag{1}$$

N_1 denotes the number of turns of the primary winding and l_{mag} the effective magnetic path length of the sample. The current leads to an alternating magnetic flux within the sample. This induces a voltage $u_2(t)$ in the high-impedance secondary winding, which is used to calculate the polarization.

$$J(t) = -\frac{1}{N_2 \cdot A_{\mathrm{mag}}} \int u_2(t)\mathrm{d}t - \mu_0 \cdot H(t) \tag{2}$$

N_2 is the number of turns of the secondary winding and A_{mag} is the magnetic cross-section of the sample. The first minus results from the induction law, while the second part of the term leads from $B(t)$ to $J(t)$. The structure thus corresponds to an open-circuit transformer and the principle circuit diagram is shown in Fig. 3. The assumption of a homogeneous field, which is a necessary condition for the calculations, can be assumed for ring samples with an outer diameter D and an inner diameter d if $1.25 < D/d < 1.4$ [14]. The above formulas are used to calculate the hysteresis loop $J = f(H)$. The connection of the reversal points of hysteresis loops with increasing excitation results in the magnetization curve.

Fig. 2. Printed ring samples as green bodies (top), sintered (left) and equipped with primary and secondary windings (right)

B. Test bench

The test bench for determining the magnetization characteristics consists of an analog amplifier, a measuring device including analogue-digital-converters for recording $i_1(t)$ and $u_2(t)$, and a PC for processing the measured data and performing the calculations. The test bench is controlled by a special *LabView* program. Fig. 3 shows the structure of the test bench and Fig. 4 the setup in the laboratory.

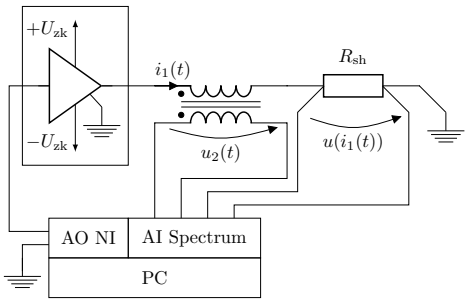

Fig. 3. Circuit diagram of the test bench

Since the relationship between field strength and polarization is nonlinear, especially in saturation, a strongly distorted current has to be supplied to generate a sinusoidal flux. Before each measurement, an estimation of the required amplifier input signal is calculated with the PC [15] and used as feed forward control, additionally an analog controller can be activated. The analog amplifier can provide high reactive power, which is mainly needed for magnetization of the sample

Authorized licensed use limited to: Middlesex University. Downloaded on September 03,2020 at 02:46:27 UTC from IEEE Xplore. Restrictions apply.

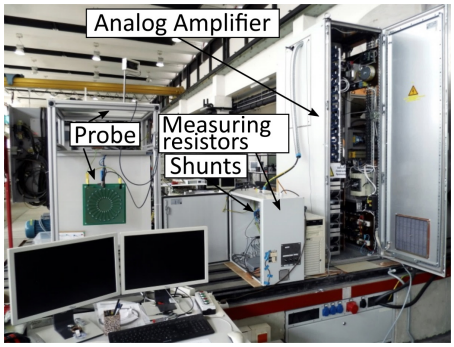

Fig. 4. Test bench, left: sample holder, middle: measuring resistors and PC, right: amplifier

into saturation. Currents up to 300 A are possible. Three measuring resistors with the values of $100\,\mathrm{m\Omega}, 10\,\mathrm{m\Omega}$ and $1\,\mathrm{m\Omega}$ allow the measurement of currents with amplitudes in the range 0.1 A to 300 A. After measuring all operating points, the magnetization curve and the specific core losses are calculated.

III. Properties at Manufacturing via 3DMMP

The novel process of 3DMMP offers the possibility to manufacture complex magnetic circuit structures in one step, if necessary using different materials, see section I.

A. development of the material

The 3DMMP process was used to produce a fully printed electric motor, see Fig. 1. The first generation of 3D-printable ferromagnetic material was used to form the magnetic circuit, which is characterized by unfavorable magnetic properties and high magnetization losses [12]. Subsequently, the development of ferromagnetic, printable materials was continued. The main challenge in context of 3DMMP is to adjust the materials in a way that the shrinkage of all combined materials is identical during sintering process. Otherwise, cracks will appear in the specimen during the heat treatment. Fig. 5 shows the magnetic properties (magnetisation curve and specific core losses) of three materials with different composition of ferromagnetic particles and ceramic. Material 1 consists of insulated iron powder with 6,25% ceramic, material 2 contains 3,25% ceramic and material 3 is only of insulated iron powder. These were produced using three different sintering regimes each, varying the sintering time. Sintering regime 2 has double and sintering regime 3 has triple time with maximum temperature of sintering regime 1. Material 1 (dark blue) shows the material used in the entirely printed motor. High ceramic content leads to a large distributed air gap, which causes a shearing of the magnetization curve. At the same time, the reduction of ferromagnetic material results in a lower saturation polarization. The curves of the magnetization characteristics and the specific losses for three sintering processes per material show that the temperature profile and the sintering time are of decisive importance. An increase in sintering time is associated with an increase of saturation flux density and a reduction of specific losses.

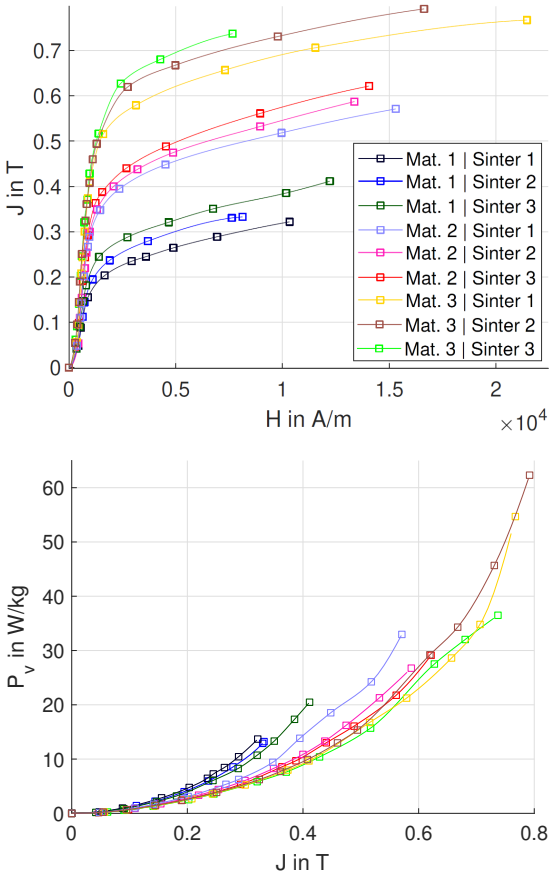
J in T
H in A/m
×10^4
Mat. 1 | Sinter 1
Mat. 1 | Sinter 2
Mat. 1 | Sinter 3
Mat. 2 | Sinter 1
Mat. 2 | Sinter 2
Mat. 2 | Sinter 3
Mat. 3 | Sinter 1
Mat. 3 | Sinter 2
Mat. 3 | Sinter 3
P_v in W/kg
J in T

Fig. 5. Development of magnetic properties of printed samples, Magnetization characteristics $J(H)$ and Specific losses $P_V(J)$ for three materials with each three sintering regimes. Measurement at 50 Hz

B. Influence of the sample geometry

To determine whether the sample geometry has an influence on the magnetic properties using 3DMMP, samples made out of a new material generation were printed with different ring widths. The maximum dimensions of the samples are limited by the printing process, but are based on the diameter ratios of the investigations on electric steel sheet samples in [16] and are listed in Tab. I. The results of the measurements are shown in Fig. 6 (Sample 1-3).

TABLE I
Dimensions of Printed Samples 1-3

Head	*Sample 1*	*Sample 2*	*Sample 3*
Outer Diameter D	$46,0\,\mathrm{mm}$	$45,3\,\mathrm{mm}$	$45,8\,\mathrm{mm}$
Inner Diameter d	$41,2\,\mathrm{mm}$	$35,8\,\mathrm{mm}$	$32,0\,\mathrm{mm}$
Diameter ratio D/d	$1,12$	$1,27$	$1,43$
Height h	$6,8\,\mathrm{mm}$	$6,8\,\mathrm{mm}$	$6,7\,\mathrm{mm}$

It is remarkable that the magnetization characteristic of the narrow sample A has the lowest saturation polarization, but a higher permeability in the region before saturation. In contrast, the widest sample has the highest saturation polarization and the lowest permeability. This characteristic is in contrast to the results of similar investigations on electric steel sheet metal

Authorized licensed use limited to: Middlesex University. Downloaded on September 03,2020 at 02:46:27 UTC from IEEE Xplore. Restrictions apply.

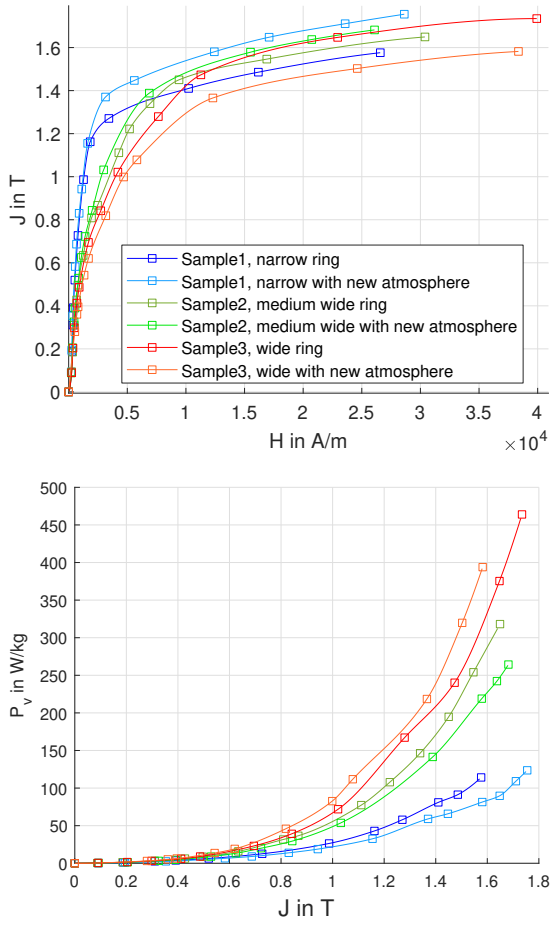

Fig. 6. Magnetic properties of printed samples with different width, measured at 50 Hz: Magnetization characteristics $J(H)$ and Specific losses $P_V(J)$

samples in [16]. There, the saturation polarization is practically not influenced by the sample width, but the magnetization characteristic is significantly lower in the range of medium polarization for narrower samples. Reason is the degradation of magnetic properties at the cutting edges of the electric steel sheets. Since no cutting of the material is required during printing, and thus neither mechanical nor thermal stresses nor lattice defects are caused in the material (these are responsible for the deterioration of the magnetic properties), no deterioration can be caused by this. The characteristic must therefore be based on the composition of the material and/or the thermal treatment.

As the described materials, used for the specimens, tended to crack in combination with ceramic and copper, material composition and sintering atmosphere were modified to improve shrinkage. Then again three samples with the same dimensions as samples 1-3 were printed and measured. The results are also shown in Fig. 6 (Sample 4-6). Comparing the curves, it is remarkable that the sample geometry influences the effect of the adapted sintering regime. The narrow sample shows a strong improvement of the magnetic properties, while the middle sized sample shows only little improvement and the wide sample even experiences a deterioration. The main focus of material development at this point was on adjusting shrinkage, so the adaption of the additives did not aim on an improvement of magnetic properties. Further more than one parameter of the process was changed from one step to another. So at this point, there is no possibility to explain the measurement results. The following discussion is intended to provide possible explanations for the measurement results, which need to be investigated further. The normalized surface to volume ratio for the ring-shaped specimen as a function of the inner diameter is shown in Fig.7. There are marks for the ratios of the three investigated samples. The ratios differ up to 33% from each other. No machining effects degrade the sample edges. Further the samples of different widths were sintered together under identical conditions. Therefore, different material properties are likely to be created during sintering due to the different sample geometries.

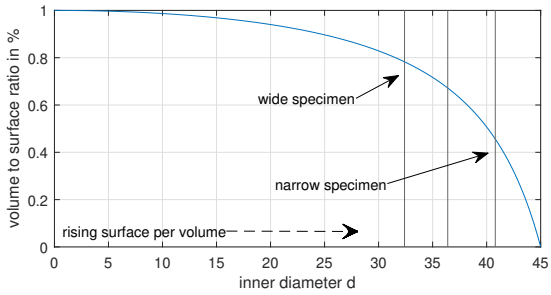

Fig. 7. Normalized ratio of volume to surface as a function of inner diameter. Actual ring specimen parameters are used for calculation.

There are some approaches to explain the results. In some cases they contradict the measurements if they are assumed separately. However, several contrary effects may occur. Therefore further series of measurements are necessary to verify or falsify these assumptions.

- All samples were exposed to the same temperature profile and the same sintering atmosphere. Since sintering proceeds from the outside to the inside, samples with a larger cross section may not have the same grade of sintering on the inside as samples with a smaller cross section. To investigate this assumption, new ring samples with the same dimensions can be sintered significantly longer at maximum temperature to see if the differences level out.
- With a larger cross-section, outer and inner areas experience different temperature curves / gradients at the heat treatment, which leads to different sintering processes inside the specimen and therefore a mixture of different material compounds. Here a microsection of the specimen cross section can be investigated.
- Flushing with gas removes separated substances during heat treatment. For narrower samples, more surface per volume is available, which allows a greater removal of separated substances. The properties of narrow samples show an improvement, i.e. the removal has a positive effect. With wide samples, however, a negative influence

Authorized licensed use limited to: Middlesex University. Downloaded on September 03,2020 at 02:46:27 UTC from IEEE Xplore. Restrictions apply.

is visible (contradiction if assumed as the only process). Measurements with different gas flushing intensity and without active gas components can be done to isolate the effect and investigate the influence.

- Surface reacts with gas (containing hydrogen (H2) as active component). With narrower samples, more surface area per volume is available, allowing more reactions on the surface. Improvement with narrow samples, i.e. influence is positive. With wide samples a negative influence can be observed, which is a contradiction. Measurements with the H2-concentration as only variable can be done to investigate the effect.

C. Comparison of hysteresis loops

The losses that occur in printed samples are much higher than those of electric steel sheets or Soft Magnetic Composites (SMC). Therefore the hysteresis loops are compared, which are a reference for the magnetization losses. For comparison, the measurement results of the narrow printed sample are used (light blue in Fig. 6). Fig. 8 shows a comparison between the hysteresis loops of the printed material, two representative SMC materials (*Fluxtrol A* and *IronPowder*) and electric steel sheets of type *M330-35A* at different excitation. The hysteresis loops of the printed materials show a strong hysteresis. In the area below saturation in Fig. 8 (top and center) a noticeable rounding of the hysteresis loops in the area of the reversal points is visible, indicating a strong eddy current development [17]. The remanence induction for high excitations, see Fig. 8 (bottom) is at $1,25\,\mathrm{T}$ and the coercive field strength at $1.75\,\mathrm{kA/m}$, which according to [18] is roughly comparable to steel 1.8159 (51CrV4) or half-hard magnetic Vacozet200 (85Co-Ni-Fe). The characteristic is much harder than with conventional electric steel. Since the breakdown of the hysteresis loop below remanence induction already starts at low negative field strengths, the material has no significant hard magnetic properties. Since the characteristic is not soft magnetic, the classification would be halfhard magnetic material. In combination with the high coercivity, the hysteresis loop has a rectangular shape. The enclosed area is therefore large and the associated losses are very high.

For *low excitation levels* the field strength requirement for 3DMMP and both SMCs is similar, but significantly higher than for soft magnetic metal sheets. The hysteresis loops of the SMC samples are wider than for electric steel sheets, which corresponds to the information in [18]. In comparison, the hysteresis loop of 3DMMP is again significantly wider. In *medium excitation levels* the hysteresis loop for 3DMMP is almost rectangular, but the field strength requirement is much lower than for SMC. The difference to electric steel sheets is mainly the significant widening of the hysteresis loop. At *high excitation level* the saturation polarization of 3DMMP is similar to that of the SMC material type *IronPowder*, but the required field strength is much lower. The saturation polarization is lower than of electric steel. The hysteresis loop is mainly rectangular, but the covered area of the ascending branch in the saturation region is very small in comparison. The majority of losses therefore occurs during the magnetization process in the medium excitation range before the material saturates.

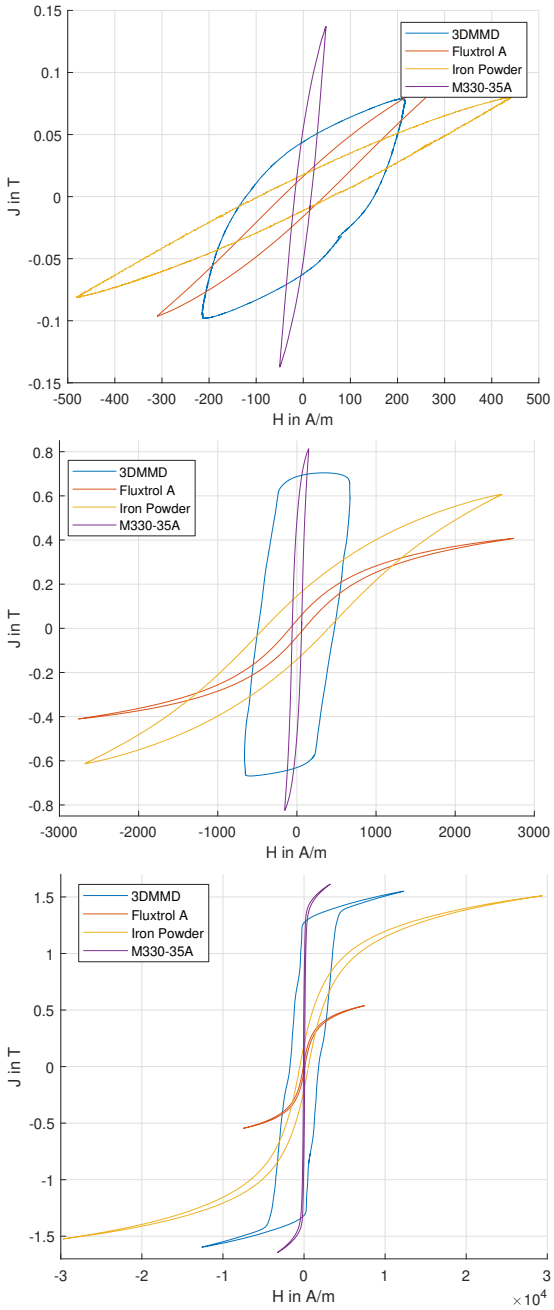

Fig. 8. Comparison of 3DMMP, two different SMC materials and electric steel sheets, measured at 50 Hz - very low excitation(top), medium excitation(center), high excitation(bottom)

D. Conclusions for further development of the material

The significant factor influencing the magnetization losses of the printed material is the high coercivity. According to [18], higher hysteresis losses occur in SMC materials than in electrical steel sheet, since the fine particles result in small ferromagnetic domains. Since the ferromagnetic components

Authorized licensed use limited to: Middlesex University. Downloaded on September 03,2020 at 02:46:27 UTC from IEEE Xplore. Restrictions apply.

of printed materials also consist of powder materials, this conclusion can also be applied to 3DMMP and is consistent with the observations of the measurements. The finer the powder, the greater the hysteresis losses. However, the hysteresis loops presented are much wider than with SMC materials, so there is potential for improvement here. One approach would be the reduction of contaminants, which have a negative effect on the coercivity, such as carbon, oxygen or sulphur [19]. In contrast, the eddy current losses are lower the finer the powder is. However, this statement only applies if the particles are electrically insulated from each other. Since high eddy current losses occur with 3DMMP, the insulation between the magnetic particles is probably defective. In the further development process, work will be done to maintain the particle insulation even during the sintering process. Due to the significance of the losses, a strong influence can be expected here. Another approach is the systematic investigation of the influence of the specimen geometry. A series of measurements with multiple samples is planned to vary both process parameters and sample geometry.

IV. Summary and Outlook

The use of printed magnetic circuits has to be considered in the context of high-temperature applications or special machine geometries that are difficult or impossible to produce by conventional techniques. 3DMMP offers the opportunity to produce complete electromagnetic structures of several materials that can withstand extremely high temperatures [10] [11] [12]. In particular, the high flexibility in production and the freedom of design are a positive aspect in relation to the less favourable magnetic properties compared to conventional SMC materials. The measurements in this paper show the development of the magnetic properties of printed ferromagnetic material, see Fig. 9. The saturation polarization is very high compared to conventional SMC materials, but does not reach the level of commercially available electrical steel. Despite enormous improvements of the losses, they are significantly increased compared to SMC materials or soft magnetic electrical steel. This is mainly due to the wide hysteresis loop with high coercive field strength. In addition to the further improvement of the material properties, future research work will focus on the advantageous use of design freedom for designing high performance electromagnetic circuits.

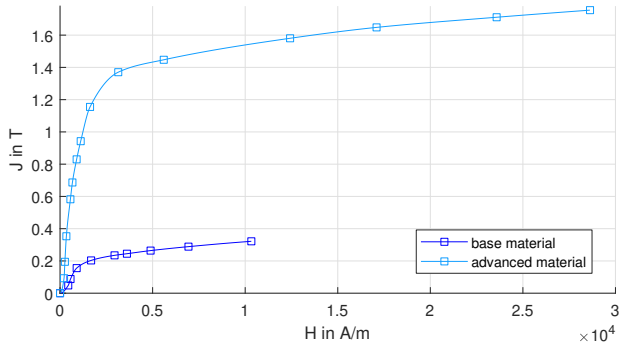

Fig. 9. Magnetisation curves of 3DMMP - comparison of development

References

[1] Z. Zhang, K. J. Jhong, C. Cheng, P. Huang, M. Tsai and W. Lee, "Metal 3D printing of synchronous reluctance motor," 2016 IEEE International Conference on Industrial Technology (ICIT), Taipei, 2016, pp. 1125-1128, doi: 10.1109/ICIT.2016.7474912

[2] T. Pham, T. Do, P. Kwon, S. Foster, "Additive Manufacturing of High Performance Ferromagnetic Materials", 2018, 4303-4308, doi: 10.1109/ECCE.2018.8558245.

[3] T. Q. Pham et al., "Binder Jet Printed Iron Silicon with Low Hysteresis Loss," 2019 IEEE International Electric Machines & Drives Conference (IEMDC), San Diego, CA, USA, 2019, pp. 1045-1052., doi: 10.1109/IEMDC.2019.8785256

[4] Yi Yan, K. D. T. Ngo, Yuhui Mei and Guo-Quan Lu, "Additive manufacturing of magnetic components for power electronics integration," 2016 International Conference on Electronics Packaging (ICEP), Sapporo, 2016, pp. 368-371., doi: 10.1109/ICEP.2016.7486849

[5] Y. Chivel, "New Approach to Multi-material Processing in Selective Laser Melting", 2016, Physics Procedia. 83. 891-898. , doi: 10.1016/j.phpro.2016.08.093.

[6] M. Ott, M.F. Zaeh, "Multi-material processing in additive manufacturing", 21st Annual International Solid Freeform Fabrication Symposium - An Additive Manufacturing Conference, SFF 2010. 195-203.

[7] G. Gotter, "Erwärmung und Kühlung elektrischer Maschinen", Springer-Verlag Berlin Heidelberg, 1954, doi: 10.1007/978-3-642-50337-5

[8] K.-D. Linsmeier, "Technische Keramik", Süddeutscher Verlag onpact GmbH, 2015, ISBN: 978-3-86236-081-9

[9] D. Cozonac, S. Babicz, S. Ait-Amar-Djennad, G. Velu, A. Cavalini and P. Wang, "Study on ceramic insulation wires for motor windings at high-temperature," 2014 IEEE Conference on Electrical Insulation and Dielectric Phenomena (CEIDP), Des Moines, IA, 2014, pp. 172-175, doi: 10.1109/CEIDP.2014.6995757

[10] F. Lorenz, J. Rudolph and R. Wemer, "Design of 3D Printed High Performance Windings for Switched Reluctance Machines," 2018 XIII International Conference on Electrical Machines (ICEM), Alexandroupoli, 2018, pp. 2451-2457., doi: 10.1109/ICELMACH.2018.8506845

[11] F. Lorenz, J. Rudolph and R. Werner, "High Temperature Operation and Increased Cooling Capabilities of Switched Reluctance Machines using 3D Printed Ceramic Insulated Coils," 2018 IEEE Transportation Electrification Conference and Expo (ITEC), Long Beach, CA, 2018, pp. 400-405., doi: 10.1109/ITEC.2018.8450089

[12] J. Rudolph, N. Trnka and F. Lorenz and R. Werner, "Vollständig 3D-gedruckte geschaltete Reluktanzmaschine in Klauenpolausführung", Elektrotechnik und Informationstechnik (E&I) 2019, Vol. 136, pp. 129-134, doi: 10.1007/s00502-019-0707

[13] J Sievert, "The measurement of magnetic properties of electrical sheet steel – survey on methods and situation of standards", Journal of Magnetism and Magnetic Materials, Volumes 215–216, 2000, pp.647-651, doi: 10.1016/S0304-8853(00)00251-1

[14] IEC 60404-6:2003 Magnetic materials - Part 6: Methods of measurement of the magnetic properties of magnetically soft metallic and powder materials at frequencies in the range 20 Hz to 200 kHz by the use of ring specimens, 2003

[15] M. Lindner and R. Werner, "Hysteresis-model oriented test procedure for soft-magnetic properties of printed or laminated toroids," 2014 4th International Electric Drives Production Conference (EDPC), Nuremberg, 2014, pp. 1-8., doi: 10.1109/EDPC.2014.6984408

[16] M. Lindner, "Ermittlung der Degeneration weichmagnetischer Werkstoffe durch Trennverfahren und ihre Berücksichtigung im Kontext elektrischer Maschinen", Dissertation 2018, urn:nbn:de:bsz:ch1-qucosa2-325897

[17] G. Bertotti, "Hysteresis in Magnetism", 1998, Academic Press Limited, ISBN: 978-0-12-093270-2

[18] R. Boll (bearb.), "Weichmagnetische Werkstoffe", 1990, Vacuumschmelze GmbH, ISBN: 3-8009-1546-4

[19] S. Cedighian, "Die magnetischen Werkstoffe", 1973, VDI-Verlag Düsseldorf, ISBN: 3-18-40 0234-9

Authorized licensed use limited to: Middlesex University. Downloaded on September 03,2020 at 02:46:27 UTC from IEEE Xplore. Restrictions apply.